

---

# DeepMI: A Mutual Information Based Framework For Unsupervised Deep Learning of Tasks

---

**Ashish Kumar**

Department of Electrical Engineering  
Indian Institute of Technology  
Kanpur, 208016  
krashish@iitk.ac.in

**Laxmidhar. Behera**

Department of Electrical Engineering  
Indian Institute of Technology  
Kanpur, 208016  
lbehera@iitk.ac.in

## Abstract

In this work, we propose an information theory based framework “DeepMI” to train deep neural networks (DNN) using Mutual Information ( $\mathcal{MI}$ ). The DeepMI framework is especially targeted but not limited to the learning of real world tasks in an unsupervised manner. The primary motivation behind this work is the insufficiency of traditional loss functions for unsupervised task learning. Moreover, directly using  $\mathcal{MI}$  for the training purpose is quite challenging to deal because of its unbounded above nature. Hence, we develop an alternative linearized representation of  $\mathcal{MI}$  as a part of the framework. Contributions of this paper are three fold: *i)* investigation of  $\mathcal{MI}$  to train deep neural networks, *ii)* novel loss function  $\mathcal{L}_{LMI}$ , and *iii)* a fuzzy logic based end-to-end differentiable pipeline to integrate DeepMI into deep learning framework. We choose a few unsupervised learning tasks for our experimental study. We demonstrate that  $\mathcal{L}_{LMI}$  alone provides better gradients to achieve a neural network better performance over the cases when multiple loss functions are used for a given task.

## 1 Introduction

The deep learning based approaches involve minimizing a similarity metric between ground truth and predictions in a way or another. Though, the way it is performed may vary from task to task. For example, the visual perception tasks such as image classification [7, 33], image segmentation [20, 37], it is performed using cross entropy whereas other tasks as forecasting [26], image generation[11], disparity/depth estimation [10], it is performed using  $\mathcal{L}_2$ ,  $\mathcal{L}_1$  metrics. Apart from that, generative adversarial [11] based learning algorithms also largely depends on the choice of similarity metric.

In the area of machine vision, there are certain tasks for which groundtruth can be not be obtained easily due to very high cost of measurement devices. These tasks include depth/disparity estimation using images, visual/LiDAR odometry [21]. These tasks are undeniably important from the perspective of the autonomous vehicles and robotics. For this reason, development of unsupervised learning techniques for these tasks have recently gained attention[10, 36, 23, 1]. The proposed methods in this direction so far, extensively use similarity metric minimization between various information sources.

From the above discussion, it is evident that similarity metric is quite crucial in the learning process. In general,  $\mathcal{L}_1$ ,  $\mathcal{L}_2$  are the most preferred choice for this purpose. Despite, their popularity, these losses do not provide desired results in many cases. It is mainly due to the fact that these are pointwise operators and do not account for statistical information while matching. For example, in images,  $\mathcal{L}_1/\mathcal{L}_2$  loss penalizes the neural network on a per pixel basis. Thus, the statistical properties are left unaccounted. To address this issue, Structural Similarity (SSIM) index [35] has recently become popular and is used as an alternative to  $\mathcal{L}_1$ ,  $\mathcal{L}_2$ . The SSIM index is computed over a window instead of a pixel and is based on local statistics. However, applicability of SSIM is limited only to images.

In practice, the aforementioned losses are used in conjunction with each other which increases the number of individual loss functions, leading to an increased complexity in order to tune the contribution of each loss [16].

Keeping in mind the above limitations, in this work, we explore the potential of  $\mathcal{MI}$  [19, 5, 32] to train deep neural networks for supervised/unsupervised learning of a task.  $\mathcal{MI}$  is essentially an information theoretic measure to reason about the statistical independence of two random variables. An interesting property of  $\mathcal{MI}$  is that it operates on probability distributions instead of the data directly. Therefore,  $\mathcal{MI}$  does not depend on the signal type i.e. images or time-series and proves to be a powerful measure in many areas. For this reason, we consider  $\mathcal{MI}$  as a potential alternative measure of similarity. Despite, its diverse applications, the expression of  $\mathcal{MI}$  is infeasible to be used directly for the training a neural network (Sec. 3). However, the interesting properties of  $\mathcal{MI}$  encourage us to dive deep into the problem and lead us to contribute through this paper as follows:

- Feasibility of  $\mathcal{MI}$  formulation for deep learning tasks.
- An  $\mathcal{MI}$  inspired novel loss function  $\mathcal{L}_{LMI}$ .
- DeepMI: a fuzzy logic based framework to train DNNs using  $\mathcal{L}_{LMI}$  or  $\mathcal{L}_{MI}$ .

In the next section, we discuss the related work. In Sec. 3, we brief  $\mathcal{MI}$  and in Sec. 4, we discuss the limitations of regular  $\mathcal{MI}$  expression and develop  $\mathcal{L}_{LMI}$  along with gradient calculation required for back propagation. In Sec. 5, we experimentally verify the importance of DeepMI through a number of unsupervised learning tasks. Finally, Sec. 6 provides conclusion about the paper.

## 2 Related Work

Literature on Mutual Information is diverse and vast. Therefore, we limit our discussion only to the most relevant works in this area. Mutual Information [32, 5, 19] is a fundamental measure of information theory which provides a sense of independence between random variables. It has been widely used in variety of applications. The works [34, 25] are typical examples which exploit  $\mathcal{MI}$  in order to align medical images.  $\mathcal{MI}$  has been successfully used in speech recognition [2] as well.  $\mathcal{MI}$  also finds its application in machine vision and robotic applications. [27] is a typical example in the area of autonomous vehicles to register 3D points clouds obtained by LiDARs. Apart from that,  $\mathcal{MI}$  has also been used in independent component analysis [14], key feature selection [22, 28]. From the above applications of  $\mathcal{MI}$  into diverse area,  $\mathcal{MI}$  can be thought as a pivotal measure.

The works [34, 25, 27] are non-parametric approaches which maximize  $\mathcal{MI}$  to achieve the desired purpose.  $\mathcal{MI}$  is operated upon distributions of the raw signals or the features extracted. For example, [34] used image histograms whereas [27] uses the distributions of 3D points in a voxel. In these techniques the feature extraction is quite important which is handcrafted. In the current decade, deep neural network architectures [12, 33] have been proved to be excellent in learning high quality embeddings/feature from the input data in entirely unsupervised manner which in turn are used for various tasks [38, 9, 30, 13, 24, 37, 11]. Therefore, we believe that bringing deep learning framework in conjunction with  $\mathcal{MI}$  can be extremely useful. However, so far, there does not exist any unified standard framework which can be used for this purpose. It is mainly due to the issues related with  $\mathcal{MI}$ . For example, the distributions required for mutual information are not exact, instead they are only the approximations of the true distribution [6]. Also, these approximations are not differentiable, thus making it difficult for  $\mathcal{MI}$  to be included in the deep learning methods [3]. Since, affordable deep learning based methods has only recently emerged, the learning process is mostly based on the traditional losses [16, 10, 36, 23, 1]. A very recent work [3] proposes to use  $\mathcal{MI}$  with neural networks. However, the work mainly addresses to estimate the distributions using neural networks and does not talk about per-sample  $\mathcal{MI}$  which is required for the tasks such as [34, 25, 27].

The recent works [10, 36, 23, 1, 4] in the area of depth estimation and visual odometry using deep neural networks in an unsupervised fashion are typical examples where  $\mathcal{MI}$  can be employed. These works only utilize the losses such as  $\mathcal{L}_1$ ,  $\mathcal{L}_2$ ,  $\mathcal{L}_{SSIM}$ . We believe that since  $\mathcal{MI}$  has successfully been employed in diverse applications, need of a well defined and benchmarked  $\mathcal{MI}$  based framework for deep learning is evident. The above discussion can be thought as a motivation for the work in this paper.

### 3 Mutual Information ( $\mathcal{MI}$ )

For any two random variables  $X$  and  $Y$ , the measure  $\mathcal{MI}$  is defined as.

$$\mathcal{I}(X; Y) = \mathcal{H}(X) + \mathcal{H}(Y) - \mathcal{H}(X, Y), \quad \mathcal{I}(X; Y) \geq 0 \quad (1)$$

$$\mathcal{H}(X) = - \sum_{x \in X} p_X^x \log(p_X^x), \quad \mathcal{H}(Y) = - \sum_{y \in Y} p_Y^y \log(p_Y^y), \quad \mathcal{H}(X, Y) = - \sum_{x \in X} \sum_{y \in Y} p_{XY}^{xy} \log(p_{XY}^{xy}) \quad (2)$$

where  $\mathcal{H}(X)$ ,  $\mathcal{H}(Y)$  represent the entropy [32] of  $X$ , entropy of  $Y$  whereas  $\mathcal{H}(XY)$  represents the joint entropy of  $X, Y$  when both variables are co-observed. While  $p_X, p_Y$  and  $p_{XY}$  represent the marginal of  $X$ , marginal of  $Y$  and joint probability density function (pdf) of  $X, Y$  respectively.

Mutual Information is an important term in the information theory. It provides a measure of statistical independence between two random variables. In other words,  $\mathcal{MI}$  governs that how well one can explain about a random variable  $X$  after observing another random variable  $Y$  or vice-versa. The expression of  $\mathcal{MI}$  in Eq. 1 is defined in terms of entropies. For any random variable  $X$ , its entropy quantifies uncertainty associated with its occurrence.

#### 3.1 $\mathcal{MI}$ as a similarity metric

$\mathcal{MI}$  is a convex function and attains global minima when any two random variables under consideration are independent. Mathematically,  $\mathcal{MI} \rightarrow 0$  when the variables are independent whereas  $\mathcal{MI} \rightarrow \{\mathcal{H}(X) = \mathcal{H}(Y)\}$  when both the variables are identical statistically. This property of  $\mathcal{MI}$ , therefore can readily be employed to quantify similarity between two signals. However, while doing so, the definition of  $\mathcal{MI}$  has to be interpreted in a quite different manner.

To better understand, let us consider an example of image matching, given two images  $X$  and  $Y$ . In order to measure the similarity between two images using  $\mathcal{MI}$ , the image itself can not be considered as a random variable. Because in that case,  $p_X, p_Y$  and  $p_{XY}$  shall be meaningless. In other words, per sample  $\mathcal{MI}$  is not defined. Hence, instead of an image, its pixel values are considered as a random variable over which the relevant distributions are defined. The pixel values may refer to intensity, color, gradients etc. In order to compute similarity, first the marginals and joint pdfs over the selected variable are computed and then similarity can be obtained by using the Eq. 1. While doing so, Eq. 2 needs to be rewritten as given below.

$$\mathcal{H}(X) = - \sum_{i=1}^N p_X^i \log(p_X^i), \quad \mathcal{H}(Y) = - \sum_{i=1}^N p_Y^i \log(p_Y^i), \quad \mathcal{H}(X, Y) = - \sum_{i=1}^N \sum_{j=1}^N p_{XY}^{ij} \log(p_{XY}^{ij}) \quad (3)$$

Where  $N$  is the number of bins in the pdf.

As an another example, we can consider matching of two time series signals by using  $\mathcal{MI}$ . As per the previous explanation, the two signal instances under consideration can not be considered as random variables, instead their instantaneous values are considered as random variable. It must be noticed that the choice of random variable depends on the application.

### 4 DeepMI Framework

Consider the image reconstruction task using autoencoders. In order to minimize the gap between the input image and the reconstructed image, clearly the  $\mathcal{MI}$  has to be maximized. The regular  $\mathcal{MI}$  expression however, can not be used directly for this purpose. It is primarily because  $\mathcal{MI}$  attains global minima when both random variables are dissimilar and our optimal point which is  $\sup \mathcal{MI}$ , is not well defined as  $\mathcal{MI}$  is unbounded above. Although, various normalized versions of  $\mathcal{MI}$  have also been proposed [29], the previously discussed issues however, persists with the normalized versions as well. Hence, normalized  $\mathcal{MI}$  ( $\mathcal{NMI}$ ) also does not serve our purpose. The above challenges encourage us to develop linearized mutual information  $\mathcal{LMI}$  which attains a global minima when the two images are exactly the same. In order to achieve this, we turn towards the working of the  $\mathcal{MI}$  and make a following important insight.

#### 4.1 A key insight to MI

Consider two images  $X$  and  $Y$ , with  $p_X, p_Y$  and  $p_{XY}$  as their marginals and joint pdfs respectively. The dimensions of  $p_X, p_Y$  is  $N \times 1$  whereas it is  $N \times N$  for  $p_{XY}$ . From, Eq. 1, 2, we can immediately say that  $\mathcal{MI} \rightarrow 0$  when two signals are dissimilar while  $\mathcal{MI} \rightarrow \{\mathcal{H}(X) = \mathcal{H}(Y)\}$  when the signals exactly the same. Hence, for the images  $X$  and  $Y$  to be identical, the necessary but not sufficient condition is that  $p_X$  and  $p_Y$  should be same. While, in order to guarantee, the following has to be satisfied.

$$p_X^i = p_Y^i = p_{XY}^{ii}, \quad p_{XY}^{ij}_{i \neq j} = 0, \quad i, j = 1, 2, \dots, N \quad (4)$$

In other words, when  $X \equiv Y$ , the off-diagonal elements of  $p_{XY}$  are zero while diagonal elements are non-zero and equals to  $p_X$  and  $p_Y$  simultaneously. The above insight leads us to derive an expression for the  $\mathcal{LMI}$  function.

#### 4.2 $\mathcal{LMI}$ Derivation

We know that for any probability density function Eq. 5 and 6 holds. These equations represent a 1D and a 2D probability density function respectively.

$$\sum_{i=1}^N p_X^i = \sum_{i=1}^N p_Y^i = 1, \quad (5)$$

$$\sum_{i=1}^N \sum_{j=1}^N p_{XY}^{ij} = 1 \quad (6)$$

Rewriting Eq. 6 as combination of its diagonal ( $i = j$ ) and off-diagonal elements ( $i \neq j$ ), we get

$$\sum_{i=1}^N \sum_{\substack{j=1 \\ i \neq j}}^N p_{XY}^{ij} + \sum_{i=1}^N p_{XY}^{ii} = 1 \quad (7)$$

$$\sum_{i=1}^N \sum_{\substack{j=1 \\ i \neq j}}^N p_{XY}^{ij} + \sum_{i=1}^N p_{XY}^{ii} + \sum_{i=1}^N p_{XY}^{ii} - \sum_{i=1}^N p_{XY}^{ii} = 1 \quad (8)$$

$$\sum_{i=1}^N \sum_{\substack{j=1 \\ i \neq j}}^N p_{XY}^{ij} + \sum_{i=1}^N p_{XY}^{ii} + \sum_{i=1}^N p_{XY}^{ii} - \sum_{i=1}^N p_{XY}^{ii} + \sum_{i=1}^N p_X^i - \sum_{i=1}^N p_X^i + \sum_{i=1}^N p_Y^i - \sum_{i=1}^N p_Y^i = 1 \quad (9)$$

$$\sum_{i=1}^N \sum_{\substack{j=1 \\ i \neq j}}^N p_{XY}^{ij} + \sum_{i=1}^N |p_{XY}^{ii} - p_X^i| + \sum_{i=1}^N |p_{XY}^{ii} - p_Y^i| - \sum_{i=1}^N p_{XY}^{ii} + 1 + 1 \geq 1 \quad (10)$$

$$\sum_{i=1}^N \sum_{\substack{j=1 \\ i \neq j}}^N p_{XY}^{ij} + \sum_{i=1}^N |p_{XY}^{ii} - p_X^i| + \sum_{i=1}^N |p_{XY}^{ii} - p_Y^i| - \sum_{i=1}^N p_{XY}^{ii} + 1 \geq 0 \quad (11)$$

Now, referring to Eq. 7, we can write

$$\sum_{i=1}^N p_{XY}^{ii} \leq 1 \quad \Rightarrow \quad 1 - \sum_{i=1}^N p_{XY}^{ii} \geq 0 \quad (12)$$

Using the above into Eq. 11, we get

$$\mathcal{L}_{LMI} = \frac{1}{3} \left( \sum_{i=1}^N \sum_{\substack{j=1 \\ i \neq j}}^N p_{XY}^{ij} + \sum_{i=1}^N |p_{XY}^{ii} - p_X^i| + \sum_{i=1}^N |p_{XY}^{ii} - p_Y^i| \right) \geq 0 \quad (13)$$

Where the factor  $1/3$  is included to ensure  $\mathcal{LMZ} \leq 1$ . It is obtained by replacing each of the three terms to their maximum. The equality of the equation to 0 will hold iff  $p_X^i = p_Y^i = p_{XY}^{ij}$ ,  $p_{XY}^{ij} = 0 \forall i, j \in 1, 2, \dots, N$ . i.e. two images match perfectly. Hence, the L.H.S. of the equation Eq. 13 is treated as the objective function which we call the  $\mathcal{LMZ}$  function. The ‘‘L’’ stands for ‘‘linearized’’ which arises because the  $\mathcal{LMZ}$  formulation is linear in the elements of pdfs. Whereas the ‘‘MI’’ term arises because at the equality, the regular  $\mathcal{MI}$  expression will also be maximized. The  $\mathcal{LMZ}$  formulation is quite interesting because it is essentially a combination of three different losses weighted equally. The  $\mathcal{L}_{LMI}$  formulation is much simpler and the gradients are easier to compute.

### 4.3 Fuzzy Probability Density Function

The  $\mathcal{LMZ}$  function utilizes the pdfs  $p_X, p_Y$  and  $p_{XY}$  which are discrete in nature. These are typically obtained by computing an  $N$ -bin histogram followed by a normalization step with  $\|\cdot\|_1 = 1$ . As per the standard procedure to compute a regular histogram, first, a bin id corresponding to an observation of the random variable is computed and later, the count of the bin is incremented by one. The computation of bin id is carried out by a *ceil* or *floor* operation which is not differentiable. While performing the rounding step, the actual contribution of the observation is lost. Thus, both the incremental and rounding procedure prevent the gradient flow which is needed during the training process.

To better understand, Let  $h_X$  be an  $N$  bin histogram of the random variate  $X$  and  $x \in X$  be an observation. In case of a regular histogram, the bin id  $x_b$  corresponding to  $x$  is computed as follows.

$$x_b = \frac{\hat{x}}{bin\_res}, \quad \hat{x} = \frac{x - min_X}{max_X - min_X}, \quad bin\_res = \frac{max_X - min_X}{N} \quad (14)$$

where  $max_X, min_X$  are the maximum and minimum values which the variable  $X$  can attain at any instant. Typically for 8-bit images,  $[min_X, max_X] = [0, 255]$ . From Eq. 14, it can be noticed that the  $x_b$  is not necessarily an integer. In this case,  $x_b$  is rounded to nearest integer by using *ceil*  $\equiv \lceil x_b \rceil$  or *floor*  $\equiv \lfloor x_b \rfloor$ , depending upon one’s convention. Now, the count of  $x_b$  is incremented by one. Therefore, it becomes evident that the rounding procedure and the unit incremental procedure do not allow the gradient computation w.r.t. the observations. To cope up with this, we employ fuzzy logic in order to ensure valid gradients during back-propagation.

#### 4.3.1 Fuzzification of $p_X$ and $p_Y$

In order to fuzzyfy  $h_X$ , instead of one as in Eq. 14, we compute two bins corresponding to  $x \in X$  i.e.  $x_0 = \lfloor x_b \rfloor$  and  $x_1 = \lceil x_b \rceil$ . We define a membership function for each of the two bins as follows.

$$m_{x_0} = 1 - (x_b - x_0), \quad m_{x_1} = (x_b - x_0) \quad (15)$$

where  $m_{x_0}, m_{x_1}$  are the membership functions of  $x_0$  and  $x_1$ . Essentially,  $m_{x_0} + m_{x_1} = 1$ . While performing the unit incremental step, the count of the bins  $x_0$  and  $x_1$  are incremented by  $m_{x_0}$  and  $m_{x_1}$  respectively instead of increasing by one. With the help of fuzzification, it can be inferred that now the gradients of  $x_b$  w.r.t.  $m_{x_0}$  and  $m_{x_1}$  are fully defined (Sec. 4.4). The above steps are followed in order to compute  $p_X$  and  $p_Y$  while the normalization being performed at the end. As a matter of convention, the memberships corresponding to  $y_b$  for a  $y \in Y$  are denoted by  $m_{y_0}$  and  $m_{y_1}$ .

#### 4.3.2 Fuzzification of $p_{XY}$

The case of joint pdf  $p_{XY}$  is simply an extension of previous steps. For a regular 2D histogram, the unit incremental procedure is applied to the bin location defined by the coordinate  $(x_b, y_b)$  (Eq. 14) which in this case as well, need not to be exactly an integral value. Therefore, to ensure valid gradient flow in this case, four memberships are defined which corresponds to the four coordinates above-left, above-right, below-left and below-right w.r.t  $(x_b, y_b)$ . Mathematically, these coordinates are given as  $(x_0, y_0), (x_1, y_0), (x_0, y_1)$ , and  $(x_1, y_1)$  and their respective memberships are given by:

$$m_{x_0 y_0} = m_{x_0} m_{y_0}, \quad m_{x_1 y_0} = m_{x_1} m_{y_0}, \quad m_{x_0 y_1} = m_{x_0} m_{y_1}, \quad m_{x_1 y_1} = m_{x_1} m_{y_1} \quad (16)$$

While performing the unit incremental step, the count of the four bins mentioned above is incremented by their respective membership value.

#### 4.4 Back-propagation through DeepMI framework

The end goal of this step is to compute gradient of an observation  $x$ . From the Eq. 16, it can be inferred that, gradient of  $x$  w.r.t.  $\mathcal{L}_{LMI}$  depends on  $p_X^{x_0}, p_X^{x_1}, p_{XY}^{x_0y_0}, p_{XY}^{x_0y_1}, p_{XY}^{x_1y_0}, p_{XY}^{x_1y_1}$ . Therefore, we can write:

$$\frac{\partial \mathcal{L}}{\partial x} = \sum_{i=0}^1 \frac{\partial \mathcal{L}}{\partial p_X^{x_i}} \frac{\partial p_X^{x_i}}{\partial x} + \sum_{i=0}^1 \sum_{j=0}^1 \frac{\partial \mathcal{L}}{\partial p_{XY}^{x_i y_j}} \frac{\partial p_{XY}^{x_i y_j}}{\partial x} \quad (17)$$

Using chain rule:

$$\frac{\partial p_X^{x_i}}{\partial x} = \frac{\partial p_X^{x_i}}{\partial \hat{p}_X^{x_i}} \times \frac{\partial \hat{p}_X^{x_i}}{\partial m_{x_i}} \times \frac{\partial m_{x_i}}{\partial x_b} \times \frac{\partial x_b}{\partial \hat{x}} \times \frac{\partial \hat{x}}{\partial x}, \quad p_X^{x_i} = \frac{\hat{p}_X^{x_i}}{\sum_{i=1}^N \hat{p}_X^{x_i}} \quad (18)$$

and similarly,

$$\frac{\partial p_{XY}^{x_i y_j}}{\partial x} = \frac{\partial p_{XY}^{x_i y_j}}{\partial \hat{p}_{XY}^{x_i y_j}} \times \frac{\partial \hat{p}_{XY}^{x_i y_j}}{\partial m_{x_i y_j}} \times \frac{\partial m_{x_i y_j}}{\partial m_{x_i}} \times \frac{\partial m_{x_i}}{\partial x_b} \times \frac{\partial x_b}{\partial \hat{x}} \times \frac{\partial \hat{x}}{\partial x}, \quad p_{XY}^{x_i y_j} = \frac{\hat{p}_{XY}^{x_i y_j}}{\sum_{i=1}^N \hat{p}_{XY}^{x_i y_j}} \quad (19)$$

Each of the above partial derivatives can be easily computed using the Eq. 13 - 16 via chain rule. It must be noticed that in the gradient calculations,  $x_0, x_1$  does not occur which would have been there in case of regular histograms leading to undefined derivatives. Similarly, gradients can be also be computed for an observation  $y$ .

#### 4.5 Hyper-parameters

The DeepMI framework has  $N$  as the only hyper-parameter. The number of bins  $N$  mainly depicts that how precisely the  $\mathcal{L}_{LMI}$  should penalize the network while matching. For example, consider an 8-bit image with dynamic range  $[0, 255]$ . Now, we set  $N = 255$ , the network will be penalized very strongly while matching. While if the  $N$  is set to a small number, the network will be forced to focus only on the important details. This property can be quite useful in cases where two images from different cameras need to be matched while both the images have different brightness levels.

## 5 Experiments

In this section, we benchmark the effectiveness and applicability of the DeepMI framework. We define three tasks on which a deep neural network is trained in an unsupervised manner. The three tasks vary in their difficulty levels from baseline, moderate, to extremely difficult from the learning perspective. As an experimental study, the training of each task is performed using different loss functions  $\mathcal{L}_1, \mathcal{L}_2, \mathcal{L}_{SSIM}$  along with  $\mathcal{L}_{MI}$  and  $\mathcal{L}_{LMI}$ . It must be noted that  $\mathcal{L}_{MI}$  and  $\mathcal{L}_{LMI}$  shares the common DeepMI framework for the training process. For  $\mathcal{L}_{SSIM}$ , we use a  $3 \times 3$  block filter following [10]. All the performance metrics are provided in Table-1 and Table-2 for quantitative analysis with the best scores highlighted in the blue. For training, we use base learning rate = 0.001, learning rate policy=*poly*, *ADAM* optimizer with  $\beta_1 = 0.9$  and  $\beta_2 = 0.99$  unless otherwise stated. The encoder-decoders [31] have a filter size of  $3 \times 3$  and number of filters 16, 32, 64, 128, 256 for the five stages for each task.

### 5.1 Unsupervised Bar Alignment (*Exp*<sub>1</sub>)

This experiment consists of two binary images where the second image is a spatially transformed version of the first i.e. a 2D rigid body transform is defined between the two images. Both the images consist of a black background and a white rectangular bar. The bar sized of  $50 \times 125$  in an image ( $192 \times 640$ ) has two degrees-of-freedom (DoF):  $tx$ , and  $\theta$  which correspond to horizontal motion and in-plane rotation. The goal of the experiment is to learn the 2DoF parameters in an unsupervised manner. For the training purpose, we generate a dataset of 1500 images with 1000+500 train-test split. The dataset is generated by transforming the bar in the image by randomly generating  $tx \in [-100, 100]$  pixels and  $\theta \in [-40, 40]$  degrees. The training of this experiment is performed using *SGD* with nesterov momentum = 0.95 for 5 epochs.

The unsupervised training pipeline for the task is depicted in Fig. 1a. While training, the neural network takes two images source ( $I_s$ ) and target ( $I_t$ ) as input and predicts  $tx, \theta$ . The image  $I_s$

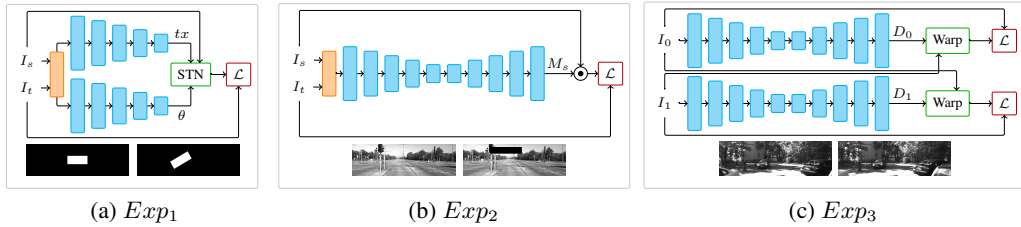


Figure 1: Unsupervised learning framework for each of the three tasks. The blue box is a convolutional block, orange box is a concatenation block. STN [15], Warp [10] and  $\mathcal{L}$  is a loss function.

Table 1: Quantitative analysis

$\mathcal{L}$	$Exp_1$		$Exp_2$					$Exp_3$
	$MAE_{tx}$	$MAE_{\theta}$	$IoU_{.05}$	$IoU_{.10}$	$IoU_{.20}$	$IoU_{.40}$	$IoU_{.50}$	$MAE(m)$
$\mathcal{L}_1$	1.52	3.44	.48	.61	.65	.68	.68	105.46
$\mathcal{L}_2$	1.93	3.65	.66	.68	.68	.68	.68	39.78
$\mathcal{L}_{SSIM}$	1.25	3.95	.50	.52	.68	.69	.81	.46
$\mathcal{L}_{SSIM} + \mathcal{L}_2$	—	—	—	—	—	—	—	.64
$\mathcal{L}_{MI}$	1.24	3.58	.68	.68	.68	.68	.68	.60
$\mathcal{L}_{LMI}$	1.04	3.18	.70	.70	.71	.80	.81	.27

is then warped ( $\hat{I}_s$ ) using fully differentiable spatial-transformer-networks (STN) [15] and  $\hat{I}_s$  is obtained. Now, the neural network is penalized using back-propagation to force  $\hat{I}_s \rightarrow I_t$ . In the testing phase, the neural network predicts  $tx, \theta$  on the test data and Mean-Absolute-Error (MAE) is reported between the predictions and the groundtruth  $tx, \theta$  which are stored during data generation process. From the Table-1 under the column  $Exp_1$ , it can be noticed that the network trained using  $\mathcal{L}_{LMI}$  formulation exhibits better performance as compared to the rest of the loss functions.

## 5.2 Unsupervised Mask Prediction ( $Exp_2$ )

This experiment consists of two ordinary grayscale images: source ( $I_s$ ) and target ( $I_t$ ). From the image  $I_t$ , a significantly large rectangular region is cropped out and filled with zeros. The end goal of the experiment is to predict a mask  $M_s$  which depicts similar and dissimilar regions between  $I_s$  and  $I_t$ . To achieve this, a neural network is trained in an unsupervised manner. For the learning process, we generate a dataset of 1500 images with 1000 + 500 train-test split. The dataset is generated by randomly cropping a rectangular region from  $I_s$  and filling the cropped region with zeros. The obtained image is referred as  $I_t$ . The cropping region has a size of  $40 \times 200$ .

Fig. 1b shows the the unsupervised training framework for this task. We use UNet [31] network architecture. The network is trained to predict  $M_s$  such that  $I_s * M_s \rightarrow I_t$ . This experiment is essentially a binary segmentation task, therefore, we adopt intersection-over-union metric (IoU) which is widely used to quantify the segmentation performance. In order to best evaluate different training losses, we provide IoU scores by thresholding the predicted mask at different confidence levels. It is done in order to examine the network’s capability to push the feature embeddings of similar and dissimilar regions significantly apart. In other words, a perfectly trained network will exhibit same IoU scores at various threshold levels. From the Table-1 under  $Exp_2$ , it is clear that the proposed  $\mathcal{L}_{LMI}$  formulation shows consistent and better performance over the other loss functions across various thresholding levels.

## 5.3 Unsupervised Depth Estimation ( $Exp_3$ )

Depth estimation has been a long standing task in front of computer vision community. This task has worldwide industrial importance because depth perception is a must for autonomous robotics and vehicles. Due to advancement in supervised learning techniques, researchers have developed several methods to predict depth using neural networks by employing supervised learning techniques.

Table 2: Effect of bin size  $N$  on  $\mathcal{L}_{LMI}$ 

$N$	$Exp_1$		$Exp_2$					$Exp_3$
	$MAE_{tx}$	$MAE_{\theta}$	IoU <sub>.05</sub>	IoU <sub>.10</sub>	IoU <sub>.20</sub>	IoU <sub>.40</sub>	IoU <sub>.50</sub>	$MAE(m)$
3	1.04	3.18	.41	.51	.52	.50	.81	.41
11	0.89	2.69	.50	.59	.61	.66	.81	.27
15	0.78	2.89	.66	.67	.68	.69	.81	.28
25	0.99	4.36	.47	.48	.58	.79	.79	.29

However, obtaining accurate groundtruth for supervised learning of this task is extremely challenging because it requires very expensive measurement instruments such as LiDARs. Hence, this task has gained considerable amount of attention in recent years in order to develop unsupervised learning frameworks for this task. The existing methods make use of several loss functions in order to learn the depth effectively.

In this experiment, We demonstrate the learning of a neural network for depth estimation using stereo images in an unsupervised manner. We form the the first ever work for this task [10] as ur basis. Our aim is not to show improvements in the datasets, instead we emphasis that how the DeepMI framework can be easily integrated for these real world applications. Hence, instead of a bigger dataset, we use 87 grayscale rectified stereo images from KITTI [8] sequence-113.

The framework to carryout the experiment is shown in Fig. 1c. It must be noticed that instead of the three different losses as in [10], we only use one loss for the evaluation. This is done in order to demonstrate that  $\mathcal{L}_{LMI}$  provides stronger gradients and alone can lead to improved results. We report MAE between predicted depth and groundtruth measurements. From the Table-1 under  $Exp_3$ , we can notice that the neural network trained using  $\mathcal{L}_{LMI}$  outperforms other five variants by large margin. For the case of  $\mathcal{L}_1, \mathcal{L}_2$ , the base learning rate is lowered to 0.00001 to prevent gradient explosion.

#### 5.4 A unified discussion on the experiments

From the Table-1, it can be noticed that the information theory based measures are much more consistent as compared to the other losses. Also, it can be noticed that for  $Exp_3$ , the  $\mathcal{L}_{LMI}$  proves to be better over the case when  $\mathcal{L}_{SSIM}$  and  $\mathcal{L}_2$  are used together. Also, it is noticeable that  $\mathcal{L}_{LMI}$  shows consistent and best scores amongst all variants of losses. This clearly marks the potential of information theory based methods in deep learning for real world applications.

#### 5.5 Effect of number of bins $N$

Table-2 shows the effect of the hyperparameter  $N$  on each of the three tasks. For  $exp_1$ , it can be noticed that the performance for all the four values of  $N$  is same. It has to be the case because the images are binary in this task. Whereas, for  $Exp_2$ , there is considerable drop in the performance for  $N = 3$  for IoU<sub>0.05</sub> (highlighted in red). It is because, the images in this case have multiple grayscale levels and details about which can not be efficiently captured. The same is the case for  $Exp_3$  when  $N = 3$ . Overall, we can see that  $\mathcal{L}_{LMI}$  has significant advantages over other loss functions. Through our experimentations, it sufficient to keep the value of  $N \leq 25$  for a signal having dynamic range  $\in [0, 255]$ .

## 6 Conclusion

In this paper, we proposed an end-to-end differentiable framework ‘‘DeepMI’’ and a novel similarity metric  $\mathcal{LMZ}$  to train deep neural networks. The metric is mutual information ( $\mathcal{MI}$ ) inspired and cops up with the difficulty to be able to train a deep neural network using the ( $\mathcal{MI}$ ) expression. The metric is based on probability density functions which makes it signal agnostic. The density functions are discrete in nature for real world signals (images, time series) and can not support backpropagation. Therefore, a fuzzification strategy to support smooth backward gradient flow through the density functions is also developed. We show that the neural network trained using  $\mathcal{L}_{MI}$  metric, outperforms their counterparts which are trained using  $\mathcal{L}_1, \mathcal{L}_2, \mathcal{L}_{SSIM}$ . Additionally, we also show that it can be easily integrated for real world applications.

## Broader Impact

In this work, we have laid foundations of DeepMI framework which is an effort to club the deep learning and mutual information together for real world applications. Through this work, we believe that, the learning based methods in several areas such as autonomous vehicles, robotic vision, speech/audio can be greatly benefitted in terms of the performance. The extensive experimental study in this work, can be used as a ground to develop extensions to the DeepMI framework in order to further improve the overall algorithmic performance. We also believe that inclusion of DeepMI into deep learning frameworks shall open door to new applications.

## References

- [1] Yasin Almalioglu, Muhamad Risqi U Saputra, Pedro PB de Gusmao, Andrew Markham, and Niki Trigoni. Ganvo: Unsupervised deep monocular visual odometry and depth estimation with generative adversarial networks. In *2019 International Conference on Robotics and Automation (ICRA)*, pages 5474–5480. IEEE, 2019.
- [2] Lalit Bahl, Peter Brown, Peter De Souza, and Robert Mercer. Maximum mutual information estimation of hidden markov model parameters for speech recognition. In *ICASSP’86. IEEE International Conference on Acoustics, Speech, and Signal Processing*, volume 11, pages 49–52. IEEE, 1986.
- [3] Mohamed Ishmael Belghazi, Aristide Baratin, Sai Rajeswar, Sherjil Ozair, Yoshua Bengio, Aaron Courville, and R Devon Hjelm. Mine: mutual information neural estimation. *arXiv preprint arXiv:1801.04062*, 2018.
- [4] Jiawang Bian, Zhichao Li, Naiyan Wang, Huangying Zhan, Chunhua Shen, Ming-Ming Cheng, and Ian Reid. Unsupervised scale-consistent depth and ego-motion learning from monocular video. In *Advances in Neural Information Processing Systems*, pages 35–45, 2019.
- [5] Thomas M Cover and Joy A Thomas. *Elements of information theory*. John Wiley & Sons, 2012.
- [6] Georges A Darbellay and Igor Vajda. Estimation of the information by an adaptive partitioning of the observation space. *IEEE Transactions on Information Theory*, 45(4):1315–1321, 1999.
- [7] Jia Deng, Wei Dong, Richard Socher, Li-Jia Li, Kai Li, and Li Fei-Fei. Imagenet: A large-scale hierarchical image database. In *2009 IEEE conference on computer vision and pattern recognition*, pages 248–255. Ieee, 2009.
- [8] Andreas Geiger, Philip Lenz, Christoph Stiller, and Raquel Urtasun. Vision meets robotics: The kitti dataset. *The International Journal of Robotics Research*, 32(11):1231–1237, 2013.
- [9] Ross Girshick. Fast r-cnn. In *Proceedings of the IEEE international conference on computer vision*, pages 1440–1448, 2015.
- [10] Clément Godard, Oisín Mac Aodha, and Gabriel J Brostow. Unsupervised monocular depth estimation with left-right consistency. In *Proceedings of the IEEE Conference on Computer Vision and Pattern Recognition*, pages 270–279, 2017.
- [11] Ian Goodfellow, Jean Pouget-Abadie, Mehdi Mirza, Bing Xu, David Warde-Farley, Sherjil Ozair, Aaron Courville, and Yoshua Bengio. Generative adversarial nets. In *Advances in neural information processing systems*, pages 2672–2680, 2014.
- [12] Kaiming He, Xiangyu Zhang, Shaoqing Ren, and Jian Sun. Deep residual learning for image recognition. In *Proceedings of the IEEE conference on computer vision and pattern recognition*, pages 770–778, 2016.
- [13] Kaiming He, Georgia Gkioxari, Piotr Dollár, and Ross Girshick. Mask r-cnn. *CVPR*, 2017.
- [14] Aapo Hyvärinen and Erkki Oja. Independent component analysis: algorithms and applications. *Neural networks*, 13(4-5):411–430, 2000.
- [15] Max Jaderberg, Karen Simonyan, Andrew Zisserman, et al. Spatial transformer networks. In *Advances in neural information processing systems*, pages 2017–2025, 2015.
- [16] Joel Janai, Fatma Guney, Anurag Ranjan, Michael Black, and Andreas Geiger. Unsupervised learning of multi-frame optical flow with occlusions. In *Proceedings of the European Conference on Computer Vision (ECCV)*, pages 690–706, 2018.
- [17] Yangqing Jia, Evan Shelhamer, Jeff Donahue, Sergey Karayev, Jonathan Long, Ross Girshick, Sergio Guadarrama, and Trevor Darrell. Caffe: Convolutional architecture for fast feature embedding. *arXiv preprint arXiv:1408.5093*, 2014.
- [18] Diederik P Kingma and Jimmy Ba. Adam: A method for stochastic optimization. *arXiv preprint arXiv:1412.6980*, 2014.
- [19] Solomon Kullback. *Information theory and statistics*. Courier Corporation, 1997.

- [20] Ashish Kumar and L Behera. Semi supervised deep quick instance detection and segmentation. In *2019 International Conference on Robotics and Automation (ICRA)*, pages 8325–8331. IEEE, 2019.
- [21] Ashish Kumar, James R McBride, and Gaurav Pandey. Real time incremental foveal texture mapping for autonomous vehicles. In *2018 IEEE/RSJ International Conference on Intelligent Robots and Systems (IROS)*, pages 3233–3240. IEEE, 2018.
- [22] Nojun Kwak and Chong-Ho Choi. Input feature selection by mutual information based on parzen window. *IEEE transactions on pattern analysis and machine intelligence*, 24(12):1667–1671, 2002.
- [23] Ruihao Li, Sen Wang, Zhiqiang Long, and Dongbing Gu. Undeepvo: Monocular visual odometry through unsupervised deep learning. In *2018 IEEE international conference on robotics and automation (ICRA)*, pages 7286–7291. IEEE, 2018.
- [24] Wei Liu, Dragomir Anguelov, Dumitru Erhan, Christian Szegedy, Scott Reed, Cheng-Yang Fu, and Alexander C Berg. Ssd: Single shot multibox detector. In *European conference on computer vision*, pages 21–37. Springer, 2016.
- [25] Frederik Maes, Andre Collignon, Dirk Vandermeulen, Guy Marchal, and Paul Suetens. Multimodality image registration by maximization of mutual information. *IEEE transactions on Medical Imaging*, 16(2): 187–198, 1997.
- [26] Aaron van den Oord, Sander Dieleman, Heiga Zen, Karen Simonyan, Oriol Vinyals, Alex Graves, Nal Kalchbrenner, Andrew Senior, and Koray Kavukcuoglu. Wavenet: A generative model for raw audio. *arXiv preprint arXiv:1609.03499*, 2016.
- [27] Gaurav Pandey, James R McBride, Silvio Savarese, and Ryan M Eustice. Toward mutual information based automatic registration of 3d point clouds. In *2012 IEEE/RSJ International Conference on Intelligent Robots and Systems*, pages 2698–2704. IEEE, 2012.
- [28] Hanchuan Peng, Fuhui Long, and Chris Ding. Feature selection based on mutual information criteria of max-dependency, max-relevance, and min-redundancy. *IEEE Transactions on pattern analysis and machine intelligence*, 27(8):1226–1238, 2005.
- [29] Josien PW Pluim, JB Antoine Maintz, and Max A Viergever. Image registration by maximization of combined mutual information and gradient information. In *International Conference on Medical Image Computing and Computer-Assisted Intervention*, pages 452–461. Springer, 2000.
- [30] Shaoqing Ren, Kaiming He, Ross Girshick, and Jian Sun. Faster r-cnn: Towards real-time object detection with region proposal networks. In *Advances in neural information processing systems*, pages 91–99, 2015.
- [31] Olaf Ronneberger, Philipp Fischer, and Thomas Brox. U-net: Convolutional networks for biomedical image segmentation. In *International Conference on Medical image computing and computer-assisted intervention*, pages 234–241. Springer, 2015.
- [32] Claude E Shannon. A mathematical theory of communication. *Bell system technical journal*, 27(3): 379–423, 1948.
- [33] Karen Simonyan and Andrew Zisserman. Very deep convolutional networks for large-scale image recognition. *CoRR*, abs/1409.1556, 2014.
- [34] Paul Viola and William M Wells III. Alignment by maximization of mutual information. *International journal of computer vision*, 24(2):137–154, 1997.
- [35] Zhou Wang, Alan C Bovik, Hamid R Sheikh, and Eero P Simoncelli. Image quality assessment: from error visibility to structural similarity. *IEEE transactions on image processing*, 13(4):600–612, 2004.
- [36] Huangying Zhan, Ravi Garg, Chamara Saroj Weerasekera, Kejie Li, Harsh Agarwal, and Ian Reid. Unsupervised learning of monocular depth estimation and visual odometry with deep feature reconstruction. In *Proceedings of the IEEE Conference on Computer Vision and Pattern Recognition*, pages 340–349, 2018.
- [37] Hengshuang Zhao, Jianping Shi, Xiaojuan Qi, Xiaogang Wang, and Jiaya Jia. Pyramid scene parsing network. In *Proceedings of IEEE Conference on Computer Vision and Pattern Recognition (CVPR)*, 2017.
- [38] Chenchen Zhu, Yutong Zheng, Khoa Luu, and Marios Savvides. Cms-rcnn: contextual multi-scale region-based cnn for unconstrained face detection. In *Deep Learning for Biometrics*, pages 57–79. Springer, 2017.